A role for proteolytic regulation of δ-catenin in remodeling a subpopulation of dendritic spines in the rodent brain

Received for publication, January 17, 2018, and in revised form, May 2, 2018 Published, Papers in Press, June 6, 2018, DOI 10.1074/jbc.RA118.001966

Li Yuan[‡§1], **Dipika Singh**[§], **James L. Buescher**[§], **and Jyothi Arikkath**[‡§2]

From the [‡]*Department of Pharmacology and Experimental Neuroscience and* [§]*Developmental Neuroscience, Munroe-Meyer Institute, University of Nebraska Medical Center, Omaha, Nebraska 68198*

Edited by Phyllis I. Hanson

Neural wiring and activity are essential for proper brain function and behavioral outputs and rely on mechanisms that guide the formation, elimination, and remodeling of synapses. During development, it is therefore vital that synaptic densities and architecture are tightly regulated to allow for appropriate neural circuit formation and function. δ-Catenin, a component of the cadherin–catenin cell adhesion complex, has been demonstrated to be a critical regulator of synaptic density and function in the developing central neurons. In this study, we identified forms of δ-catenin that include only the N-terminal (DcatNT) or the C-terminal (DcatCT) regions. We found that these δ-catenin forms are differentially expressed in different regions of the male mouse brain. Our results also indicated that in rat primary cortical culture, these forms are generated in an activity-dependent manner by Ca^{2+}-dependent and calpain-mediated cleavage of δ-catenin or in an activity-independent but lysosome-dependent manner. Functionally, loss of the domain containing the calpain-cleavage sites allowing for generation of DcatCT and DcatNT perturbed the density of a subpopulation of dendritic protrusions in rat hippocampal neurons. This subpopulation likely included protrusions that are either in transition toward becoming mature mushroom spines or in the process of being eliminated. By influencing this subpopulation of spines, proteolytic processing of δ-catenin can likely regulate the balance between mature and immature dendritic protrusions in coordination with neural activity. We conclude that by undergoing cleavage, δ-catenin differentially regulates the densities of subpopulations of dendritic spines and contributes to proper neural circuit wiring in the developing brain.

Mechanisms that guide formation, elimination, and remodeling of synapses are critically regulated during development to allow appropriate neural circuit wiring and function (1, 2) and behavioral outputs. Components of the cadherin–catenin cell adhesion complex have been identified to as key regulators in these processes (3). δ-Catenin is a cytosolic component of the complex and is predominantly expressed in the central nervous system (4–6). We and others have identified critical roles for the protein in synaptic and dendritic architecture and function (7–14). Mice lacking δ-catenin have impaired learning and memory (15), suggesting that δ-catenin is a critical component of the machinery underlying neural circuit formation and function. Consistently, mutations in *CTNND2*, encoding δ-catenin, have been identified in autism, and loss of *CTNND2* is associated with intellectual disability (16–18).

Proteolytic regulation is a commonly used mechanism in central neurons to allow for selective substrate cleavage leading to differential functional output, for example local or compartmentalized signaling, or allow functional roles that are different from the uncleaved forms of the protein (19–21). These mechanisms are tightly regulated and play key roles in a variety of neuronal functions, including axon guidance, neuronal excitability, and transcription, and their dysregulation has been implicated in human disease (20–22).

We have identified a novel proteolysis-based mechanism that allows δ-catenin to regulate the densities of dendritic protrusion subpopulations in developing central neurons. More specifically, we have identified novel forms of δ-catenin that include forms that are cleaved by calpain in an NMDA[3] receptor (NMDAR)-dependent manner in central neurons to generate N- and C-terminal fragments (DcatNT and -CT). Our data also demonstrate the existence of an additional activity-independent pool of CT and NT that is regulated differentially by the lysosome and the proteasome. Furthermore, we have identified a novel functional role for this cleavage in synaptic regulation. Our data indicate that the ability of δ-catenin to be cleaved is critical for the ability of δ-catenin to regulate the density of a subpopulation of dendritic protrusions in pyramidal neurons. Based on dendritic protrusion architecture, a significant portion of this subpopulation includes protrusions that

This work was supported in part by Startup Funds from the Munroe-Meyer Institute, grants from the Alzheimer's Association, The Nebraska Research Initiative, National Institutes of Health Institutional Development Award (IDeA) 5P20GM103471-10 from NIGMS, Nebraska EPSCoR Grant EPS-1004094, and National Institutes of Health Grant 1R03MH110726-01. The authors declare that they have no conflicts of interest with the contents of this article. The content is solely the responsibility of the authors and does not necessarily represent the official views of the National Institutes of Health.

This article contains Figs. S1–S4.

[1] Supported by a graduate student fellowship from the University of Nebraska Medical Center.

[2] To whom correspondence should be addressed. Tel.: 402-559-8461; E-mail: jyothi.arikkath@unmc.edu.

[3] The abbreviations used are: NMDA, *N*-methyl-D-aspartic acid; NMDAR, NMDA receptor; NT, N-terminal fragment; CT, C-terminal fragment; DcatNT, δ-catenin N terminus; DcatCT, δ-catenin C terminus; δ-cat, δ-catenin; pen-strep, penicillin-streptomycin; TTX, tetrodotoxin; Baf, bafilomycin A1; VGCC, voltage-dependent calcium channel; ANOVA, analysis of variance; CI, confidence interval; AMPAR, α-amino-3-hydroxy-5-methyl-4-isoxazolepropionate receptor; SBDP, spectrin breakdown product; DIV, days *in vitro*; TAP, tandem affinity purification; CNQX, 6-cyano-7-nitroquinoxaline-2,3-dione.

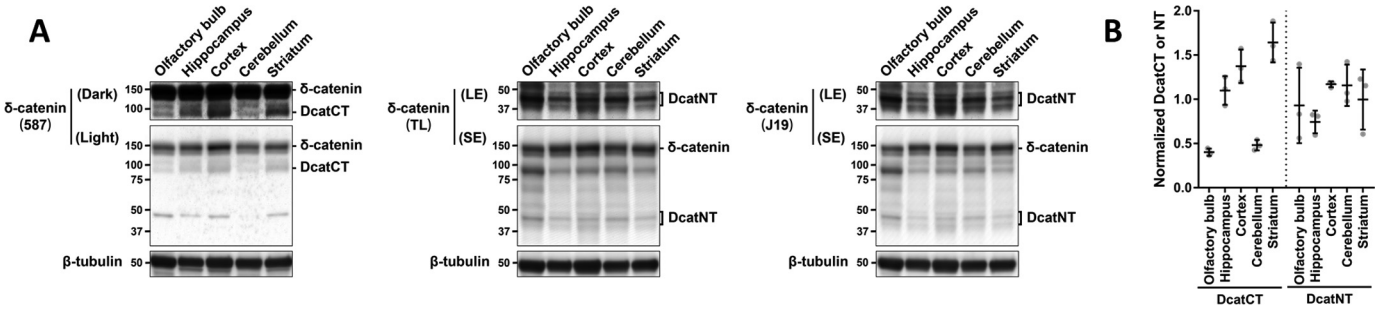

Figure 1. Expression of two novel forms of δ-catenin, DcatNT and DcatCT, in different regions of the brain. Immunoblots for δ-catenin (*A*) and quantification of DcatCT and -NT (*B*) in different brain regions in 1–2-month-old mice ($n = 3$, mean ± S.D.) are shown. The quantifications of DcaCT and -NT were done with 587 and J19 antibodies, respectively. The *top two sections* in each panel in *A* are from the same blot. The *first section* is either a long exposure (*LE*) or a dark-adjusted (*Dark*) version for better visualizing the protein with low expression. The *second section* is either a short exposure (*SE*) or a light-adjusted (*Light*) version for better visualizing the protein with high expression. DcatNT consists of two bands, above and below the strong band (nonspecific), in the *top section*. The band about 50 kDa from 587 and the band about 90 kDa from TL and J19 are nonspecific bands (see Fig. S1).

are in transition, toward elimination or maturation. Thus, proteolytic regulation of δ-catenin can coordinate with neural activity to influence the balance between mature and immature dendritic protrusions and regulate neural circuit formation in developing central neurons.

Results

Two novel isoforms of δ-catenin in the brain

We took advantage of validated anti-δ-catenin antibodies (Fig. S1, *A* and *B*) to examine localization patterns of δ-catenin in different regions of the mouse brain. In addition to full-length δ-catenin forms detected by both N- and C-terminal antibodies, we observed two bands with molecular masses in the range of 40–50 kDa that could be detected by the two different N-terminal antibodies, TL and J19, but not the C-terminal 587 antibody (Fig. 1*A*), indicating that they include the N-terminal region but not the C-terminal region of the protein. These proteins are collectively referred to as DcatNT for the δ-catenin N terminus. Similarly, we observed an ~90-kDa band that could be detected by the C-terminal antibody, but not the N-terminal antibodies (Fig. 1*A*). Moreover, this band was not detected in lysates from the δ-catenin N-terminal mouse, indicating that it is generated from the δ-catenin (Fig. S1*B*). This band is referred to as DcatCT for the δ-catenin C terminus.

The DcatNT was expressed at similar levels in different regions of the brain (Fig. 1, *A* and *B*), whereas the expression levels of DcatCT showed more regional variation with higher levels in hippocampus, cortex, and striatum compared with other regions (Fig. 1, *A* and *B*). These data indicate that multiple forms of δ-catenin that include either the N or C terminus are differentially expressed in different regions of the brain.

Generation of DcatCT via a calpain-dependent mechanism

We examined whether the DcatCT/NT forms of δ-catenin could be generated in transiently transfected HEK cells by transfecting full-length δ-catenin cDNA and immunoblot analysis (Fig. 2*A* and Fig. S2*A*). These lysates were prepared in EDTA-free buffers as indicated under "Experimental procedures." Both the DcatCT and -NT fragments could be detected in these lysates indicating that the machinery for generating DcatCT and -NT exists in HEK cells. We used this system to examine the requirement for chelators for generating DcatCT and -NT (Fig. 2*B*), because several proteases require metal ions for activity. The levels of DcatCT are sensitive to the concentration of EDTA in the buffer, indicating that the generation of DcatCT depends on metal ions. To identify the metal ion of interest, we performed similar experiments in lysates supplemented with Ca^{2+}, Mg^{2+}, or Zn^{2+}. As shown in Fig. 2*B*, the inclusion of Ca^{2+} was sufficient to restore generation of DcatCT. We suspect that the effects of Zn^{2+} are likely caused by its high affinity to EDTA (23), which then likely depletes the EDTA available to chelate Ca^{2+}. These data indicate that the generation of DcatCT depends on Ca^{2+}.

We also confirmed that the levels of DcatCT and -NT were dependent on the chelator in neurons by using a similar approach (Fig. S2, *B* and *C*). Furthermore, purified TAP-tagged δ-catenin, expressed and purified from transiently transfected HEK cells, can be cleaved to generate DcatCT when incubated with lysates from untransfected HEK cells (Fig. S2*D*) but not when the HEK lysates were heat-inactivated (Fig. 2*C*). Taken together, these results suggest that δ-catenin is cleaved to generate DcatCT by a Ca^{2+}-dependent protease that is ubiquitously expressed.

One candidate protease for Ca^{2+}-dependent cleavage is calpain, a Ca^{2+}-dependent cysteine protease (22, 24). To assess whether δ-catenin is a substrate of calpain, primary neurons were lysed in lysis buffer that included chelators and either of three calpain inhibitors, ALLN, MDL28170, and MG132, and immunoblotted to detect DcatCT. As a positive control, lysates without chelators were also included. In lysates with either of the inhibitors, but not inhibitors for proteasome and cathepsin B, lactacystin and CA-074 Me, respectively, the levels of DcatCT were decreased compared with lysates without chelators (Fig. 2, *D* and *E*), suggesting that DcatCT is generated in a calpain-dependent manner in neurons. Taken together, these results indicate that DcatCT is generated in a calpain-dependent manner in neurons.

DcatCT and -NT can be generated in an NMDAR-dependent manner by calpain-mediated cleavage

δ-Catenin is localized at synapses and regulates synaptic structure and function (9), and calpain can be activated via glutamate receptor activation (25). To assess whether the cleavage of δ-catenin can be induced by neuronal activity, we examined

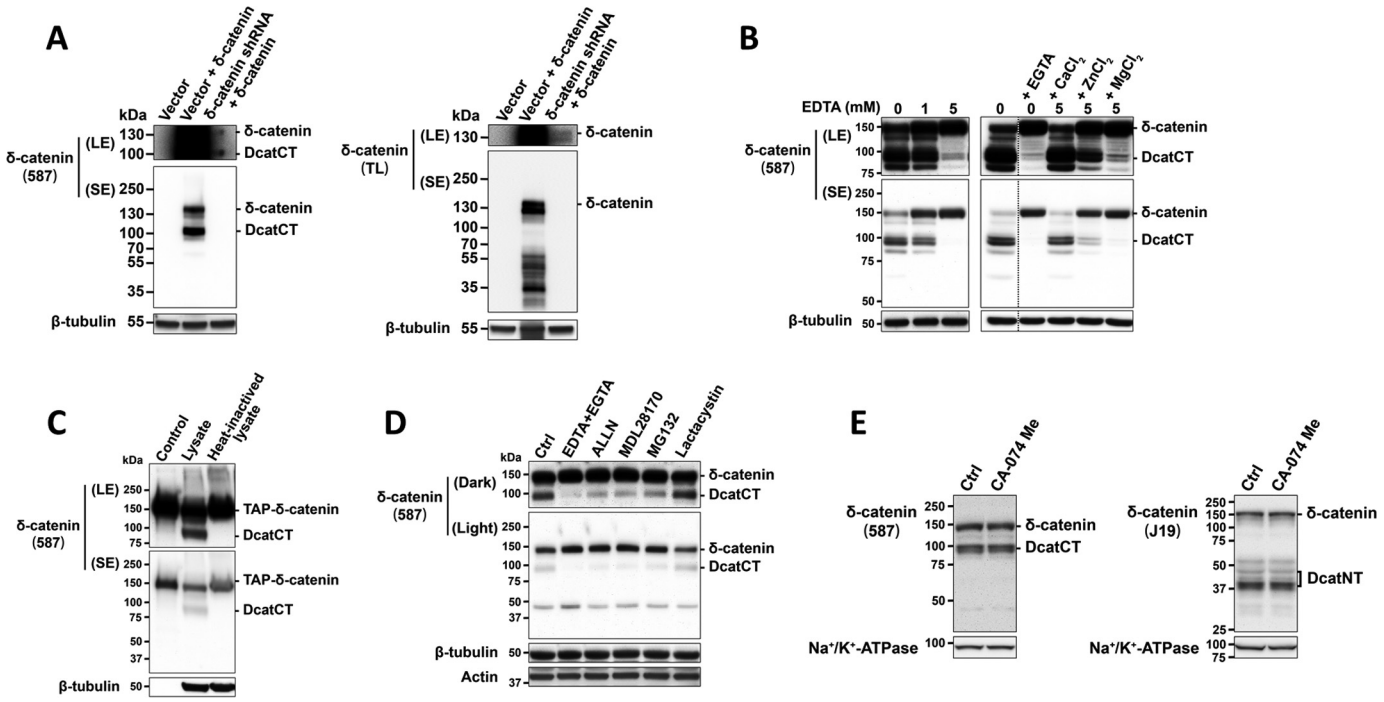

Figure 2. δ-Catenin is a substrate of calpain *in vitro*. *A,* immunoblots for DcatCT and N-terminal fragments in HEK cells transfected with δ-catenin plus vector or δ-cat shRNA ($n = 4$). *B,* immunoblots for DcatCT in lysates of δ-catenin–transfected HEK cells in the indicated buffers with the indicated dose of chelator and chelator supplemented with metal ions ($n = 3–4$). *C,* immunoblots for DcatCT from purified full-length δ-catenin (*TAP–δ-catenin*) treated with control or heat-inactivated nontransfected HEK cell lysate ($n = 3$). *D,* immunoblots for DcatCT in *in vitro* cleavage assay on cortical neurons supplemented with calpain and proteasome inhibitors (ALLN, 50 μM; MDL28170, 100 μM; MG132, 50 μM; lactacystin, 20 μM; $n = 3–4$). *E,* immunoblots for DcatCT and -NT in *in vitro* cleavage assay on cortical neurons pretreated with 5 μM CA-074 Me for 15 min ($n = 3$).

whether the ability of δ-catenin to be cleaved by calpain can be induced by glutamate treatment. Primary cortical neurons in culture treated with 20 μM glutamate for 5 min were lysed in a buffer containing chelators to avoid confounds from calpain-mediated cleavage occurring during the processing of the neurons, and the levels of DcatCT and -NT were examined by immunoblot analysis. The levels of DcatCT and -NT increased with glutamate treatment indicating that they were regulated by glutamate receptor activation and were inhibited in the presence of two NMDAR inhibitors, D-AP5 and MK801 (Fig. 3*A*). The presence of the calpain inhibitors, ALLN and MDL28170, but not the cathepsin B inhibitor CA-074 Me blocked the cleavage of δ-catenin mediated by glutamate (Fig. 3, *A* and *B*). Moreover, the activation of calpain was confirmed by the detection of the calpain cleavage product SBDP (spectrin breakdown product, indicated by * sign) in the lysates (Fig. 3, *A* and *B*). These results indicate that δ-catenin can be cleaved in an NMDAR-dependent manner by calpain to generate DcatCT and -NT.

We confirmed that the cleavage of δ-catenin is mediated by NMDAR and calpain, by using NMDA instead of glutamate (Fig. 3, *C* and *D*) and NMDAR and calpain inhibitors (Fig. 3, *E* and *F*). The NMDAR and calpain-mediated cleavage of δ-catenin was unaffected by tetrodotoxin (TTX), a voltage-dependent sodium channel blocker, nimodipine, an L-type voltage-dependent calcium channel (VGCC) blocker, ascomycin, an inhibitor for the Ca^{2+}-dependent phosphatase calcineurin, and lactacystin (Fig. 3, *E* and *F*). Furthermore, primary neurons treated with NMDA in Ca^{2+}-free extracellular media and processed as above had reduced levels of DcatCT and -NT compared with media containing Ca^{2+} (Fig. 3*G*). These studies indicate that the calpain-mediated cleavage of δ-catenin is regulated by NMDAR and requires Ca^{2+}-influx through the NMDAR.

On closer examination, similar to DcatNT, we observed that the DcatCT included two separate bands DcatCTI and -II that are very close in molecular weight (Fig. 3*H*) suggesting that there are two calpain sites within δ-catenin in close proximity to each other. Consistently, the Pearson correlation test showed that DcatCTI/II (the ratio of DcatCTI to -II) and DcatNTII/I (the ratio of DcatNTII to I) were correlated (Fig. 3*I*). Furthermore, although DcatCTI is the predominant form under basal conditions, the generation of DcatCTII is more sensitive to agonist treatment (Fig. 3*H*). There is a significant decrease in DcatCTI/II and DcatNTII/I with glutamate treatment (Fig. 3, *J* and *K*). Taken together, these data indicate that there are likely two sites of calpain cleavage on δ-catenin that differ in sensitivity to activity mediated by NMDAR activation and glutamate treatment preferentially induce cleavage at the second site.

Basal pool of DcatCT and -NT

Our data demonstrate that there is a basal pool of DcatCT and -NT in absence of externally added glutamate or NMDA (Fig. 3*H*). We sought to examine whether this pool is also dependent on NMDAR for generation in primary cortical neurons. Blocking neural activity by TTX did not affect the levels of DcatCT and -NT (Fig. 4, *A–C*). Consistent with neither calpain inhibition nor activation under these conditions, there were no differences in the levels of SBDP (Fig. 4*D*), a commonly used marker for calpain activity (22, 25), with TTX. To further confirm the dependence of the generation of the basal pool of

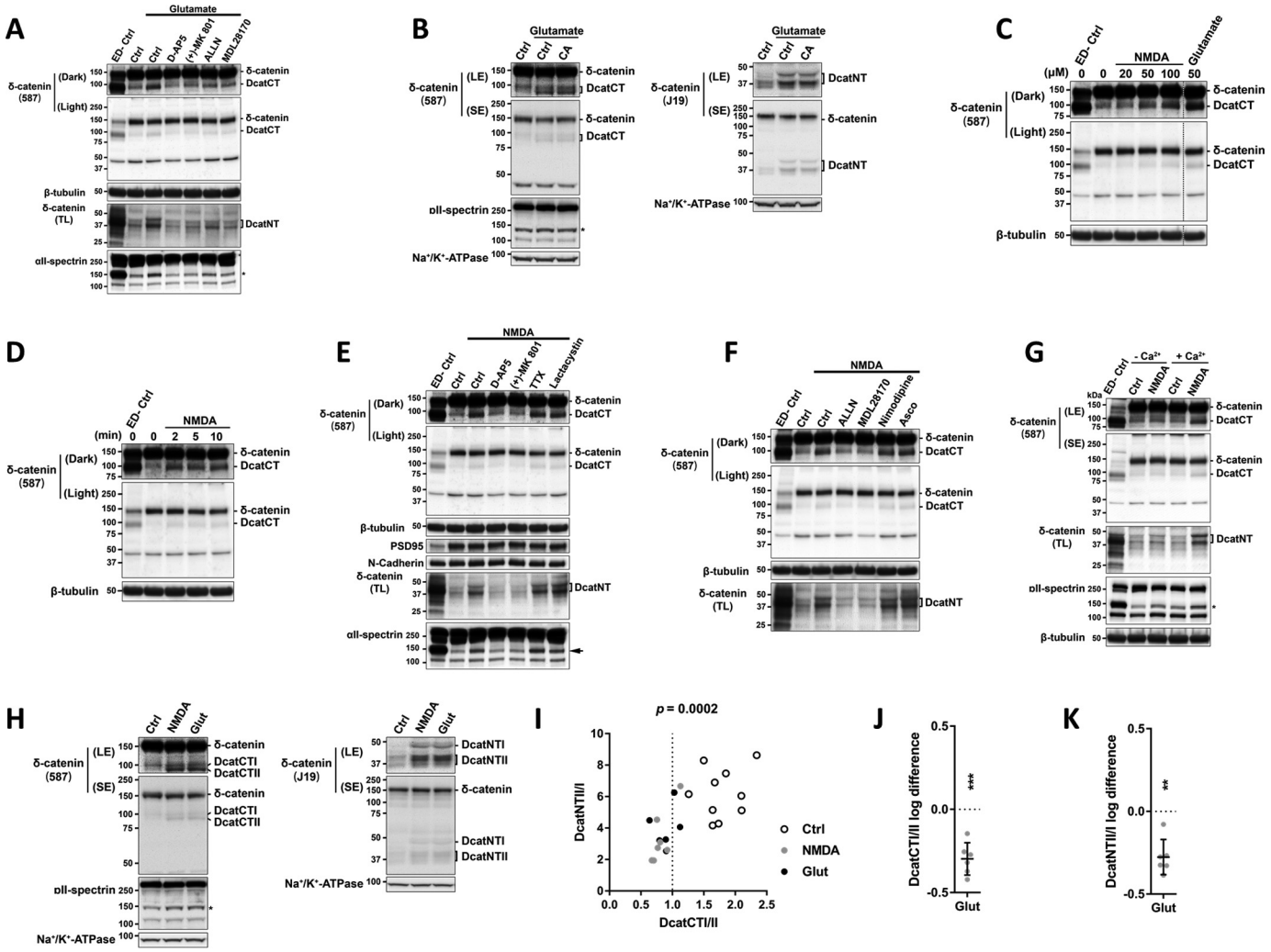

Figure 3. NMDAR-mediated Ca^{2+} influx induces δ-catenin cleavage and DcatCT/NT generation by calpain. *A* and *B*, immunoblots for DcatCT and -NT in cortical neurons treated with 20 μM glutamate for 5 min with 10-min pretreatments with NMDAR or calpain inhibitors (*D-AP5*, 100 μM; *MK801*, 10 μM; *ALLN*, 50 μM; *MDL28170*, 100 μM, $n = 3$) (*A*) or cathepsin B inhibitor (CA-074 Me, 5 μM, $n = 3$) (*B*). *C*, immunoblots for DcatCT in cortical neurons treated with the indicated dose of NMDA/glutamate for 5 min ($n = 3$). *D*, immunoblots for DcatCT in cortical neurons treated with 100 μM NMDA for the indicated lengths of time ($n = 3$). *E* and *F*, immunoblots for DcatCT and -NT in cortical neurons treated with 100 μM NMDA treatment for 5 min with pretreatments with NMDAR inhibitors, D-AP5 and (+)-MK801 (*E*) or calpain inhibitors, ALLN and MDL28170 (10 min pretreatment, TTX, 1 μM; lactacystin, 20 μM; nimodipine, 10 μM; ascomycine (*Asco*), 2 μM, $n = 3$–4) (*F*). *G*, immunoblots for DcatCT and -NT in cortical neurons treated with 100 μM NMDA for 5 min in extracellular medium with/without Ca^{2+} ($n = 3$). *H*, immunoblots for two forms of DcatCT and -NT, DcatCTI (*top*), CTII (*bottom*), NTI (*top*), and NTII (*bottom*), in cortical neurons treated with NMDA/glutamate for 5 min (NMDA, 50 μM; glutamate, 20 μM). Molecular mass for two bands of DcatCT: 97.13 ± 0.8345 and 89.63 ± 1.302 kDa, respectively ($n = 8$, mean ± S.D.). *I*, Pearson correlation of the ratio of DcatCTI/II and DcatNTII/I. These data are pooled from replicates of the data shown in *H* and *B*, control ($n = 10$), NMDA ($n = 7$), and glutamate ($n = 6$). *J* and *K*, quantification of DcatCTI/II and DcatNTII/I in the glutamate (*Glut*)-treated samples in *I* (paired *t* test, DcatCTI/II, −0.2974 ± 0.09702; DcatNTII/I, −0.276 ± 0.1061; mean ± S.D.). *ED-Ctrl*, control sample without EDTA/EGTA, as positive control of DcatCT/NT in the *in vitro* cleavage assay.

DcatCT and -NT on spontaneous NMDAR activity, primary neurons were treated with MK801. Under these conditions, there were no changes in the levels of DcatCT and -NT (Fig. 4, *E–H*). Similarly, treatment of neurons with the AMPAR inhibitor CNQX, or even CNQX and MK801 co-treatment, had no effect on the levels of DcatCT and -NT (Fig. 4, *E–H*). Our data similarly indicate that the basal levels of DcatCT and -NT are insensitive to the L-type VGCC blocker, nimodipine (Fig. 4, *M–P*). These results indicate that the basal levels of DcatCT and -NT are insensitive to NMDAR and L-type VGCC inhibition.

Because the basal levels of DcatCT and -NT could also be affected by their degradation, we examined whether blocking degradation would affect their levels. Two major cellular pathways that regulate protein degradation are the proteasome and lysosome pathways. Using approaches similar to those described above, we examined the sensitivity of basal forms of DcatCT and -NT to inhibitors of proteasome or lysosome. Lactacystin treatment significantly increased the level of DcatNT and SBDP but not CT (Fig. 4, *J* and *K*), indicating that DcatNT and SBDP are degraded by proteasome. Co-treatment of lactacystin and MK801 did not significantly alter the levels of DcatNT and SBDP compared with lactacystin control (Fig. 4, *I–K*), further confirming that the basal generation of DcatCT and -NT is NMDAR-independent (Fig. 4*E*). Consistently, no differences in the levels of DcatCT or -NT were observed with D-AP5 treatment (Fig. S3). To examine the dependence of DcatCT and -NT degradation on the lysosome, we treated primary neurons with the V-ATPase inhibitor bafilomycin A1 (Baf), which alters the intralysosomal pH (26, 27). Baf treatment

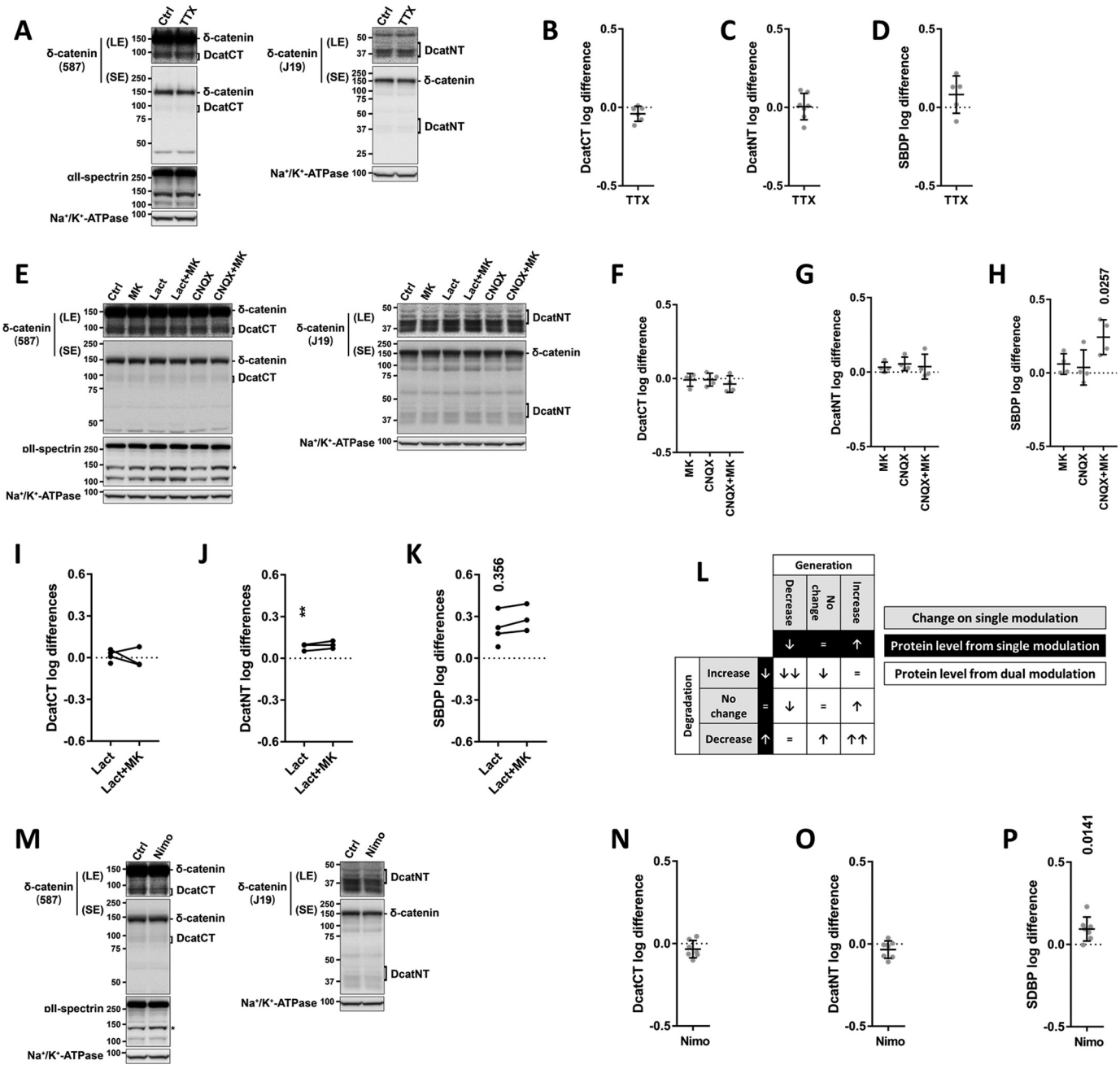

Figure 4. Basal generation of DcatCT/NT is NMDAR-independent. *A–D*, immunoblot (*A*) and quantification of DcatCT, -NT, and SBDP in cortical neurons treated with TTX for 3 h (TTX, 1 μM; paired *t* test; DcatCT, $p = 0.0982$, $n = 6$; DcatNT, $p = 0.8696$, $n = 7$; SBDP, $p = 0.1991$, $n = 5$; mean ± S.D.). *E*, immunoblot for DcatCT, -NT, and SBDP in cortical neurons treated with 3-h inhibitors of NMDAR, AMPAR, and proteasome (*MK801*, 10 μM; *CNQX*, 10 μM; lactacystin (*Lact*), 10 μM) (*B–D*). *F–H*, quantification from samples with NMDAR and AMPAR inhibitors (paired *t* test, $n = 4$, mean ± S.D.). *I–K*, quantification from samples with proteasome inhibitor (paired *t* tests: control (*Ctrl*) *versus* lactacystin, $n = 4$; *Lact versus Lact + MK*, $n = 3$). *L*, diagram of predicted changes on the levels of DcatCT/NT/SBDP based on generation and degradation. *M–P*, immunoblot (*M*) and quantification of DcatCT, -NT, and SBDP in cortical neurons treated with 3-h L-type VGCC inhibitor (*Nimo*, 10 μM; paired *t* test; DcatCT, $p = 0.1410$; DcatNT, $p = 0.1408$; $n = 7$; mean ± S.D.) (*N–P*).

did not affect the levels of DcatCT but significantly reduced the levels of NT (Fig. 5, *A–C*). These effects on δ-catenin are not a secondary consequence of cell stress and cell death, as indicated by the lack of alteration in the levels of SBDP (25) (Fig. 5*D*) in control or Baf-treated neurons or endoplasmic reticulum stress as indicated by insensitivity to thapsigargin (28), a sarco/endoplasmic reticulum Ca^{2+}-ATPase (SERCA) inhibitor (Fig. 5, *A–D*).

Furthermore, treatment of primary unstimulated neurons with MDL28170 altered the levels of DcatCT and -NT in a manner similar to the results obtained with Baf, in which the levels of DcatCT were unaltered by treatment but the levels of NT were significantly reduced (Fig. 5, *A–C*). MDL28170 inhibits the conventional calpains and cathepsin B, but there is less support to indicate that it effective inhibits atypical calpains. Under these conditions, SBDPs were also not altered in levels (Fig. 5*D*), indicating that under basal conditions the conventional calpains are not activated for the basal generation SBDP. The decreased levels of DcatNT under these conditions are consistent with a model in which MDL28170 inhibits cathepsin

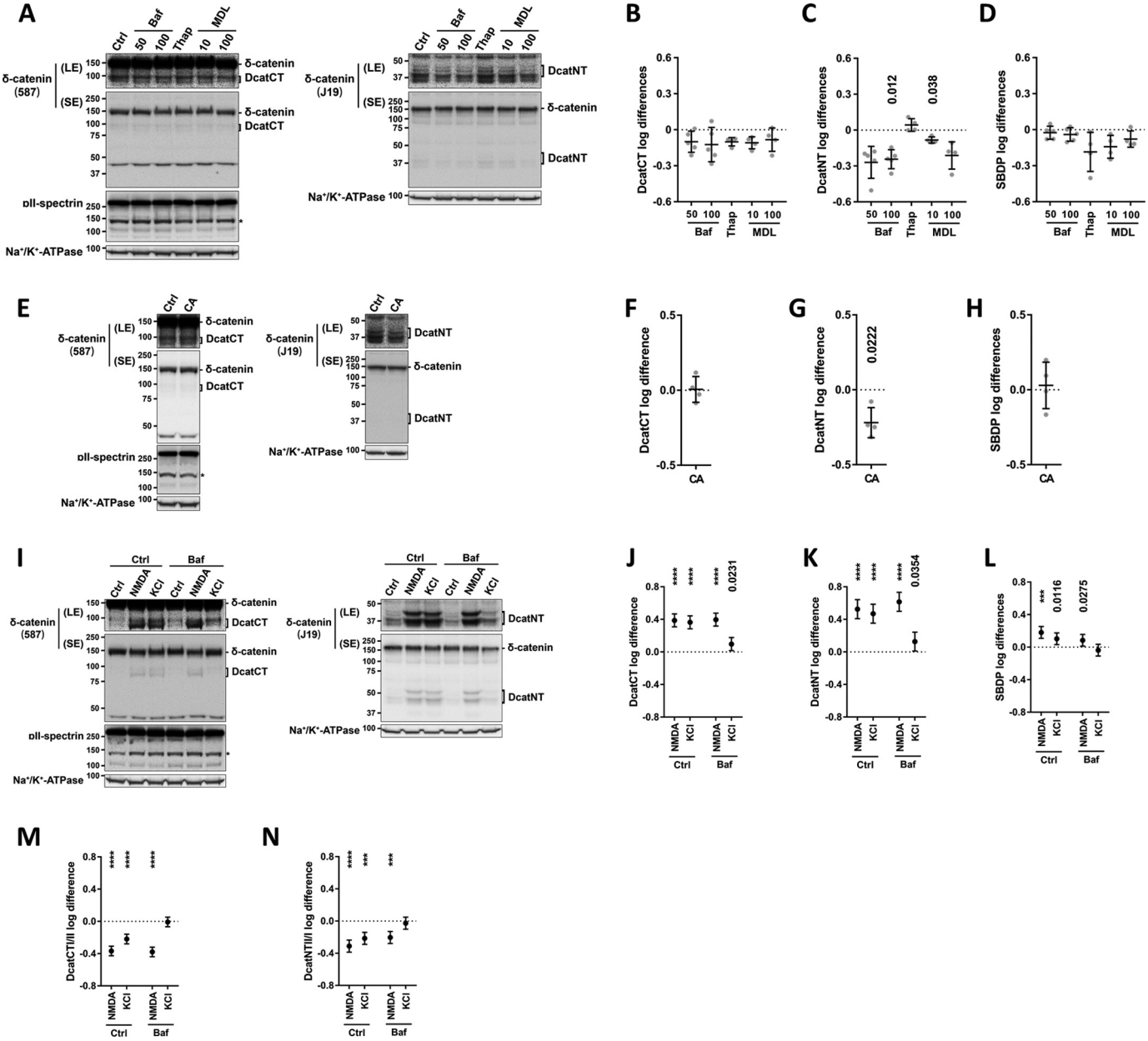

Figure 5. Lysosome dysfunction inhibits the basal generation of DcatNT. *A–D*, immunoblot (*A*) and quantification of DcatCT, -NT, and SBDP in cortical neurons treated with 3-h Baf, thapsigargin (*Thap*), and MDL28170 (*Thap,* 200 nM; *Baf,* nM, MDL28170: μM; paired *t* test with Bonferroni-Dunn's correction, $n = 4–5$, mean ± S.D.) (*B–D*). *E–H*, immunoblot (*E*) and quantification of DcatCT, -NT, and SBDP in cortical neurons treated with 3-h cathepsin B inhibitor (CA-074 Me, 1 μM; paired *t* test, $n = 4$, mean ± S.D.) (*F–H*). *I–N*, immunoblot (*I*) and quantification of DcatCT, -NT, and SBDP (*J–L*) DcatCTI/II and DcatNTII/I, in cortical neurons treated with 5 min NMDA or KCl after 3-h Baf pretreatment (*Baf,* 50 nM; NMDA, 50 μM; KCl, extra 55 mM (*M* and *N*); repeated measure two-way ANOVA, multiple comparison with the control samples of both groups with Dunnett's correction, $n = 4$, mean ± CI).

B, which in turn disrupts lysosome function, thus decreasing δ-catenin cleavage. To confirm these results, primary neurons were treated with CA-074 Me. This treatment caused a significant decrease of DcatNT but no change of DcatCT or SBDP (Fig. 5, *E–H*). Thus, the inhibition of cathepsin B is sufficient to inhibit the basal generation of NT.

These results suggest that the generation and degradation of DcatNT are dependent on lysosome and proteasome pathways, respectively. However, the levels of DcatCT are insensitive to both proteasome and lysosome inhibitors.

To assess whether the basal generation and NMDAR-dependent cleavage of δ-catenin are correlated, we examined the levels of DcatCT and -NT in neurons treated with NMDA or KCl after 3 h of Baf treatment (Fig. 5*I*). Baf had no effect on NMDAR-induced cleavage of δ-catenin and αII-spectrin (Fig. 5, *J–L*), indicating that the basal and NMDAR-dependent forms of DcatCT and -NT are generated by two independent pathways. Interestingly, with depletion of synaptic vesicle by Baf (29), KCl still managed to induce δ-catenin cleavage, but it was unable to reduce DcatCTI/II and NTII/I ratios (Fig. 5, *J–L*). Moreover, the NMDA-induced decrease of DcatCTI/II and NTII/I was significantly lower compared with KCl (Fig. 5, *M* and *N*). These results are consistent with the previous observation that NMDAR activation preferably cleaves δ-catenin at the second cleavage site (Fig. 3*H*).

Taken together, these data indicate the following: 1) there are multiple forms of DcatCT and -NT; 2) some of the DcatCT and -NT forms are generated in an NMDAR-dependent manner by cleavage of δ-catenin by calpain; 3) basal forms of DcatCT and -NT are not influenced by spontaneous NMDAR activity or Ca^{2+} influx through L-type VGCC; 4) basal forms of DcatCT and -NT are differentially regulated in terms of their generation and degradation, whereas DcatNT depends on the proteasome for degradation and lysosome for generation, the mechanisms of degradation and generation of DcatCT are insensitive to proteasome and lysosome inhibitors; and 5) basal and activity-dependent forms of DcatCT and -NT are generated by independent pathways.

Calpain-mediated cleavage of δ-catenin regulates a subset of dendritic protrusions in hippocampal neurons

Knockdown or loss of δ-catenin leads to an increase in excitatory spine density accompanied by an increase of miniature excitatory postsynaptic current frequency (8, 9, 12). We sought to examine whether calpain-mediated cleavage of δ-catenin affects the ability of δ-catenin to regulate dendritic protrusion density in hippocampal neurons. We mapped the calpain cleavage sites on δ-catenin using the *in vitro* cleavage assay in HEK cells as described above (Fig. 2, *B* and *D*, and Fig. S4, *A* and *B*). Using this information, we generated three constructs of δ-catenin that partially (DI321420 and DI391435) or completely (DI321440) blocked calpain-mediated cleavage (Fig. 6, *A* and *B*) and evaluated the ability of these constructs to rescue the protrusion density phenotype observed with knockdown of δ-catenin.

Primary hippocampal neurons were transfected with vector, shRNA to δ-catenin (δ-cat shRNA), or shRNA with either WT δ-catenin or the three calpain-resistant forms of δ-catenin (DIV 12) and fixed (DIV 18), and dendritic protrusion densities were examined by confocal microscopy (Fig. 6*C*). In neurons expressing δ-cat shRNA, there was a significant increase in the density of protrusions (Fig. 6*D*). This could be rescued by the introduction of full-length δ-catenin or the DI321420 construct. The DI391435 construct demonstrated borderline rescue, and the DI321440 did not rescue the shRNA knockdown phenotype. However, the *p* values for the partially resistant constructs are very close to being significant ($p = 0.0504$). This led us to believe that there might be population differences within the groups that might be obscuring significant data.

Dendritic protrusions vary in width and length, partly reflecting synapses at different levels of maturity or development. To assess the distribution of various groups of dendritic protrusions, we examined the protrusion population in vector-expressing neurons and classified them into three groups based on the frequency distribution of protrusion length and width (Fig. 6*E*). These groups were classified as population 1 (P1): width ≤ 0.5 μm and length ≤ 1 μm; population 2 (P2): width ≤ 0.5 μm and length > 1 μm; and population 3 (P3): width > 0.5 μm. These three populations, P1, P2, and P3, include stubby and short thin-spines or filopodia, long thin-spines or filopodia, and mushroom spines, respectively (30). We examined the distribution of dendritic protrusions in these three populations in neurons expressing vector, shRNA, or shRNA and full-length δ-catenin or calpain-resistant forms for δ-catenin (Fig. 6*F*). The density of dendritic protrusions classified into either of the three categories was increased in neurons expressing δ-cat shRNA. This effect on the P1 and P2 subpopulations could be significantly rescued by the WT δ-catenin. However, the rescue of the shRNA-mediated increase in P1 protrusion density was rescued by the DI321420 and DI391435 but not the DI321440 construct. In contrast, the DI321420 and DI321440 constructs but not DI391435 construct rescued the phenotype of δ-catenin knockdown in the P2 protrusions. These results indicate that the calpain cleavage is necessary for the ability of δ-catenin to regulate the density of the P1 protrusions. The phenotype of the P2 protrusions may be slightly more complex and may reflect incomplete or partial calpain cleavage and needs further investigation.

We further characterized the effects of the calpain-resistant form of δ-catenin on the P1 protrusions. The density of the P1 protrusions can be defined as the product of the fraction of P1 protrusions in the whole population and the dendritic protrusion density (see "Experimental procedures"). Thus, the increase in the density of P1 protrusions with knockdown of δ-catenin could be a function of increase of one or both of these parameters. To examine this relationship, we plotted the dendritic protrusion density and P1 fraction for individual neurons from each group (Fig. 6*G*). The heatmap indicates the density of the P1 protrusions in each group. In neurons expressing vector, the percentage of the P1 protrusions decreased with an increase in the density of total protrusions.

One possible explanation of this observation is that there is an upper limit to the density of P1 protrusions in individual dendrites. Thus, a threshold defined as the predicted upper limit of the density of P1 protrusions in the vector group fits the following criteria: if such a limit exists, the prediction would be as follows: 1) a threshold can be drawn with the density of P1 protrusions, and the majority of dendrites should have a density of P1 protrusions that fall below the threshold; and 2) frequency distribution of density of P1 protrusions from all the dendrites would demonstrate a nonparametric distribution, and a small population of dendrite would pass the threshold.

According to these criteria, we defined a threshold by examining the frequency distribution of the density of P1 protrusions in the vector group by bootstrapping analysis (Fig. 6*H*). This threshold defines the predicted upper limit of the density of P1 protrusions in the vector group. Thus, we define two populations of P1 density, one above and one below the threshold. Once we defined this threshold, we sought to examine whether the fraction of P1 density above the threshold differs in neurons expressing δ-cat shRNA or the different constructs described above by bootstrapping (Fig. 6*I*). In neurons expressing δ-cat shRNA, the fraction of P1 protrusions that were above the threshold were significantly increased compared with vector. This knockdown phenotype could be rescued by all the constructs, including WT δ-catenin, but not the DI321440. These results are consistent with the model in which δ-catenin regulates the upper limit of density of P1 protrusions in each neuron and mechanistically requires calpain-mediated cleavage to perform this functional role.

Discussion

In this study, we have made several important observations. 1) Multiple novel forms of δ-catenin that include only the N-terminal region (DcatNT) or the C-terminal region (DcatCT) are differentially expressed in different regions of the brain. 2) Some forms of DcatCT and -NT are generated by an NMDAR-, Ca^{2+}-, and calpain-dependent mechanism. 3) Basal forms of DactCT and -NT are insensitive to spontaneous neural activity. 4) Basal forms of DcatCT and -NT are differentially regulated. Although basal DcatNT is degraded in a proteasome- and generated in a lysosome-dependent manner, the levels of DcatCT are insensitive to proteasome and lysosome inhibitors. 5) The ability of δ-catenin to be cleaved is necessary for its ability to regulate a subpopulation of dendritic protrusions. This subpopulation of protrusions that likely represents protrusions are in transition, either toward being eliminated or maturing. Thus, by manipulating cleavage, δ-catenin can likely influence the balance between mature and immature protrusions in coordination with neural activity and strongly influence neural circuit wiring in the developing brain.

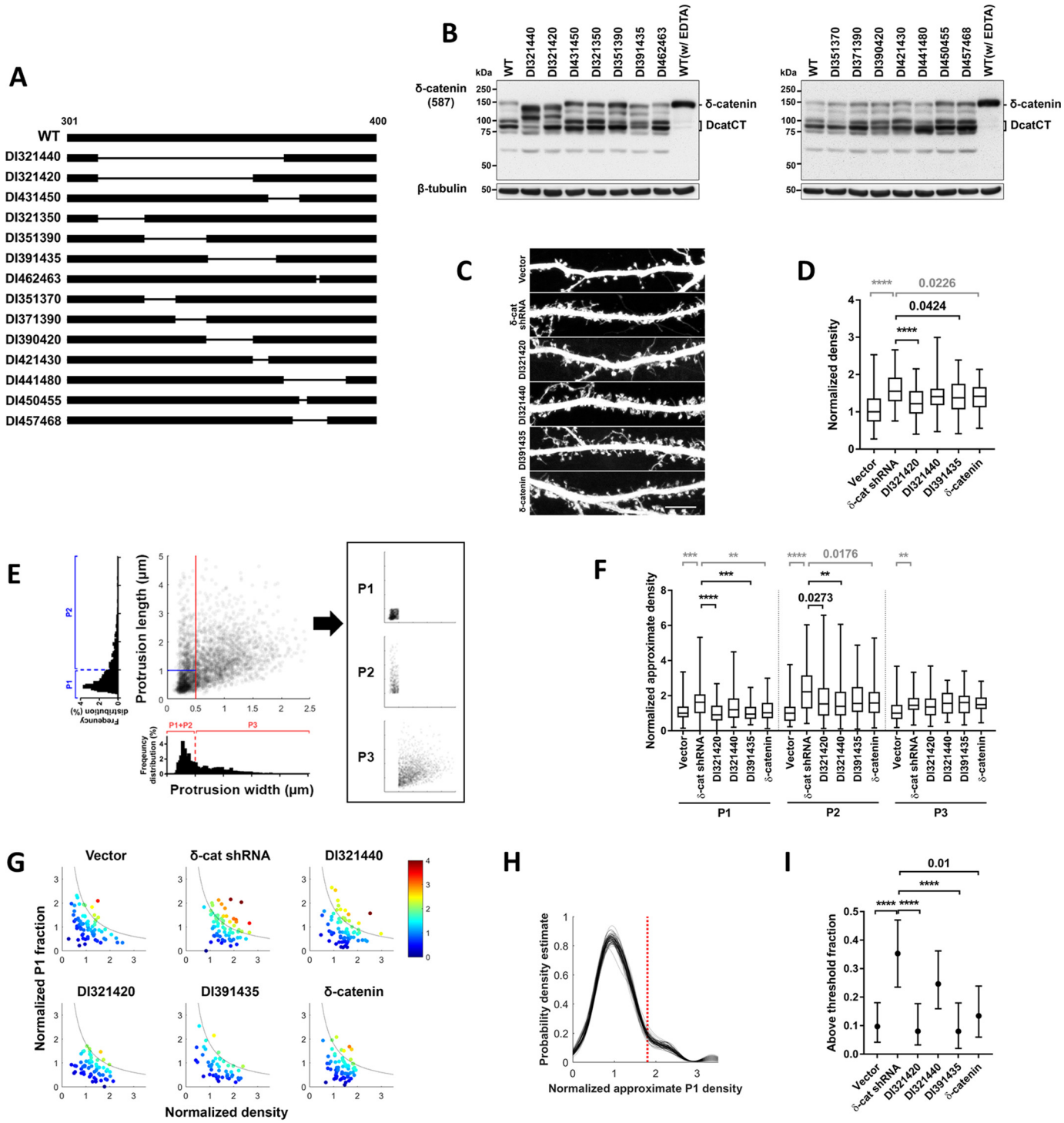

Different forms of δ-catenin

Our data demonstrate that, in addition to the full-length δ-catenin, novel forms of δ-catenin, DcatCT and -NT, are expressed differentially in different regions of the brain. While our studies have focused on the cortex and the hippocampus, the expression of these forms in different regions of the brain implies that they may have additional functional roles that may or may not be related to synaptic regulation. Our data clearly demonstrate that some forms of DcatCT and -NT are generated by calpain-mediated cleavage (Fig. 3). However, some forms of DcatCT and -NT may or may not be dependent on conventional calpain for generation (Fig. 5, *A–C*). The lysosome is an organelle that allows for protein degradation in an acidic environment. Surprisingly, our data demonstrate a role for the lysosome in generation of basal forms of DcatNT. Although lysosome-dependent degradation mechanisms are a common form of regulation to alter cellular levels of a protein (31), there are few, if any, examples of proteins that rely on the lysosome for generation. The mechanism for this is unclear.

The levels of basal DcatCT appear to be regulated independently of the levels of basal DcatNT. This suggests that basal DcatCT and -NT may have independent functional roles and mechanisms of generation/regulation. Our data do not provide a clear mechanism for generation of DcatCT. Certainly, other mechanisms that might allow the generation of these forms exist, including transcriptional, translational, or proteolytic mechanisms.

Functional roles of DcatCT and DcatNT

Our data also demonstrate that the inability to cleave δ-catenin has detrimental consequences on the density of a subset of dendritic protrusions in hippocampal neurons. However, our studies do not exclude the possibility that the two forms DcatCT and -NT have additional functional roles that are unique to each form. The C terminus of δ-catenin includes regions that are necessary for cadherin binding (9) and PDZ interactions (32–34) and a predicted NLS motif (4, 35, 36). This region also includes the palmitoylation site on δ-catenin that is key for the ability of δ-catenin to regulate synaptic plasticity (9). The C-terminal half of the protein likely also contains interaction sites for other currently unidentified proteins. Similarly, the N-terminal region of δ-catenin includes the interaction sites for the DIPA family of proteins (37). Furthermore, the cleaved DcatCT and -NT are likely structurally distinct from the full-length protein thus allowing for differential interactions with other proteins. Thus, it is certainly possible that the cleaved forms of δ-catenin have additional functional roles that are distinct from the full-length forms. The use of cleaved forms of proteins to perform functional roles that are different from the full-length protein is widely used by different cell types (20, 21, 38). Such functional roles for δ-catenin remain to be identified and are likely to be of great interest to neural circuit formation and function in the developing brain. Mutations in *CTNND2* have been identified in autism. These mutations are point mutations and span the entire protein (16). Interestingly, some of these mutations, like R454H, are located in a region that is very close to the calpain-cleavage site. It is tempting to speculate that at least some of these mutations may lead to detrimental effects on either the ability of calpain to cleave δ-catenin or, by virtue of their localization within DcatNT or -CT, lead to a functional compromise. Further studies are necessary to provide experimental evidence for this hypothesis.

Regulation of densities of subpopulations by processing of δ-catenin

Our data indicate that knockdown of δ-catenin predominantly increases the populations of the P1 group of dendritic protrusions. The increase in the density of the P1 protrusions with knockdown of δ-catenin cannot be rescued by constructs that lack the region that includes the calpain-cleavage site, suggesting that this region is necessary for the ability of δ-catenin to regulate the density of P1 protrusions (Fig. 7).

The P1 population includes stubby spines, short thin-spines, and short filopodia. The short filopodia likely represent an intermediate stage along the process of protrusion formation or elimination. Although the stubby and short thin-spines are expected to have active synapses (30, 39), the stability of both these populations requires contact-dependent mechanisms

Figure 6. δ-Catenin affects dendritic protrusion density. *A,* schematic of individual constructs of δ-catenin with indicated deletions between 301 and 400 amino acids (the numbers of the construct name reflect amino acid numbers for the deletion on mouse δ-catenin). The *thin line* between *black bars* indicates the deletion area for each construct. *B,* immunoblot for *in vitro* generation of DcatCT in HEK cells transfected with indicated δ-catenin deletion constructs ($n \geq 3$). *C,* representative images of dendritic segments from hippocampal neurons transfected with vector, δ-catenin shRNA (*δ-cat shRNA*), δ-catenin, DI321420, DI321440, and DI391435. *D,* quantification of the density of dendritic protrusion for each group. The densities were normalized to the geometric mean of the vector group in each experiment (Kruskal-Wallis test, Dunn's multiple comparison test: vector, δ-catenin shRNA, and δ-catenin (*gray*); δ-catenin shRNA, DI321420, DI321440, and DI391435 (*black*); 59–80 neurons per group from four independent experiments; median ± 25/75% (*box*) and minimum/maximum (*whisker*)). *E,* criteria for separation of dendritic protrusion into three groups. Individual dendritic protrusions from the vector group represented by a *dot* and plotted according to the width (*x* axis) and length (*y* axis) in the *top-middle panel*. The frequency distribution of the width of all the protrusions are shown in the *bottom-middle panel,* and a threshold was drawn (*red line*) to separate the protrusions into two populations, P1 + P2 and P3, according to the difference in distribution. The frequency distribution of the length of P1 + P2 is shown in the *left panel,* and a threshold was drawn (*blue line*) to separate the population into two, P1 and P2, according to the difference in distribution. The distribution of population in each of the P1–3 population is shown in the *right panel*. 3443 protrusions are from four independent experiments. *F,* quantification of the approximate density of each population of dendritic protrusions in groups indicated. The densities were normalized to the median of the vector group in each experiment (Kruskal-Wallis test and Dunn's multiple comparison test: vector, δ-catenin shRNA, and δ-catenin for all populations (*gray*); δ-catenin shRNA, DI321420 and DI321440, DI391435 for P1 and P2 (*black*). 50–72 neurons per group from four independent experiments; median ± 25/75% (*box*) and minimum/maximum (*whisker*)). *G,* relationship between the fraction of P1 protrusion and dendritic protrusion density in each group. Individual neurons from each group are represented by a *dot* and plotted according to the normalized dendritic protrusion density (*x* axis) and normalized P1 fraction (*y* axis). The normalized approximate P1 density of each neuron is indicated by heat map. The P1 fraction were normalized to the median of the vector group in each experiment (50–72 neurons per group from four independent experiments). The P1 density threshold is indicated by the *black line*. *H,* estimation of the P1 density threshold. Probability density estimates were calculated from the normalized approximate P1 density from resampling the vector group (*black line*; 72 neurons from four independent experiments), and a threshold was estimated and is indicated by a *red dotted line*. *I,* bootstrap comparison of the fraction of neurons with above threshold P1 density in groups indicated (*p* value are calculated by bootstrap paired *t* test with δ-cat shRNA, with Bonferroni-Dunn correction, 50–72 neurons per group from four independent experiments, median ± CIs).

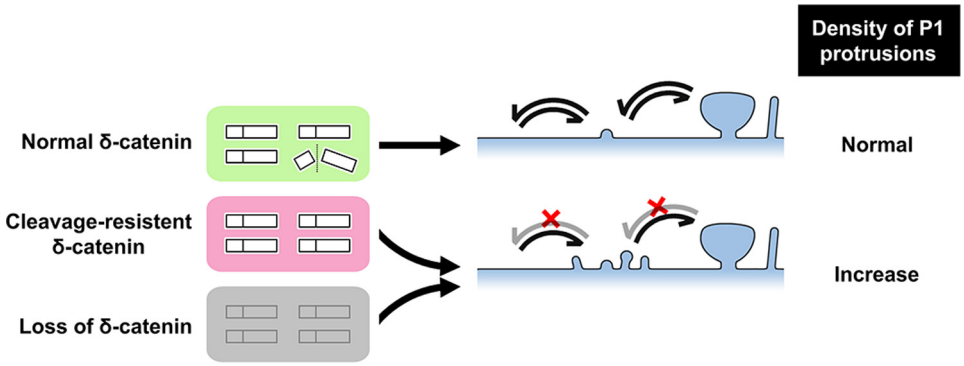

Figure 7. Model: δ-catenin is a critical regulator of excitatory dendritic protrusion density in the hippocampus. δ-Catenin can be cleaved by calpain in an activity-dependent manner to release N- and C-terminal fragments. This ability of δ-catenin to be cleaved is critical for its ability to regulate the density of the P1 protrusions that likely represent protrusions that are in transition between immature and mature protrusions. Thus, δ-catenin is a critical regulator of neural circuit formation in the developing brain.

(30, 40). This suggests that a significant fraction of the P1 subpopulation likely represents protrusions that are in transition, either toward being eliminated or being stabilized (41). Our data indicate that the cleavage of δ-catenin is linked to the upper limit of the density of P1 protrusions. This implies that neurons have an inherent mechanism to regulate the density of this class of protrusions. To do this, it is essential that the neuron has the ability to compute the density of protrusions, to evaluate whether the density of P1 protrusions is close to the upper limit, and to initiate a cascade of events that maintains the density of these protrusions. How δ-catenin participates in this computation and contributes to regulating the density of P1 protrusions is not entirely clear. We propose that processing of δ-catenin, by directly influencing the P1 subpopulation of protrusions, can likely influence the balance between mature and immature dendritic protrusions in coordination with neural activity.

As mentioned above, the bulk of the P1 protrusions likely represents an intermediate stage with their eventual fate being elimination or maturation. Although our data do not provide direct evidence for a direct functional role for cadherin-mediated regulation of these processes in the ability of δ-catenin to regulate protrusion subpopulations, it is tempting to speculate that proteolytic regulation of δ-catenin modulates its ability to interact with cadherin and influence the adhesive properties of cadherin thereby indirectly influencing synaptic contacts. Furthermore, because the cadherin–catenin complex is linked to the actin cytoskeleton (3), the alterations in the interactions between δ-catenin and cadherin could, in theory, promote signaling to the actin cytoskeleton thereby influencing protrusion density or stabilization. Similarly, because δ-catenin associated with cadherin binds to several PDZ domain-containing synaptic proteins (12), it is possible that cleavage of δ-catenin influences its association with PDZ domain scaffolding proteins thus impacting synapse assembly or disassembly.

In summary, we have identified novel forms of δ-catenin that are differentially regulated both in terms of their generation and degradation by protease-, proteasome-, and lysosome-dependent mechanisms. Furthermore, we have identified differential functional roles for calpain-mediated cleavage of δ-catenin in regulating densities of subpopulations of dendritic protrusions. Taken together with previous data (8, 9), these data suggest that δ-catenin is a critical regulator of excitatory synapses in central neurons, employs differential mechanisms to regulate densities of protrusion sub-populations, and is thus a critical regulator of neural circuit formation in the developing brain.

Experimental procedures

Animals

All experiments were approved by the University of Nebraska Medical Center Institutional Animal Care and Use Committee. Animals were housed in 12:12 dark/light cycle with free access to water and food. The δ-catenin N-terminal mouse was a generous gift from Dr. Xin Liu (UCLA) (15). Brain tissues from different regions and *in vitro* cleavage assay were collected from C57BL/6 mice. For all experiments, except for the *in vitro* cleavage assay, only male mice were used.

Cell culture and transfection

All cell cultures were incubated at 37 °C with 5% CO_2. HEK 293 cell was a generous gift from Dr. Shilpa Buch (University of Nebraska Medical Center). HEK cells were maintained in Dulbecco's modified Eagle's medium (ThermoFisher Scientific, 11965-092/SH30022.01) supplemented with 10% heat-inactivated FBS (ATLABS) and pen-strep (ThermoFisher Scientific, SV30010). Primary hippocampal and cortical cultures were prepared from E18 to E19 Sprague-Dawley rats (Charles River Laboratories), as described previously (42), with a plating density of 18,750 and 50,000 cells/cm^2, respectively. 4–6 h after plating, cells were switched to maintenance medium, containing Neurobasal Medium (ThermoFisher Scientific, 21103049), B-27 Supplement (ThermoFisher Scientific, 17504044), and pen-strep (ThermoFisher Scientific, 15070-063). For the *in vitro* assay (Fig. S2*C*), hippocampal culture was treated with mitotic inhibitor 5 μM Ara-C (Sigma, C1768) at DIV 2–4 to minimize the number of glial cells to specifically test the cleavage on neurons. Otherwise, glial cells were not excluded to mimic the physiological condition *in vivo*. Half of the media were changed every 3–5 and 2–4 days for hippocampal and cortical culture respectively.

Lipofectamine 2000 (ThermoFisher Scientific) was used for transfection according to the manufacturer's protocol. For neurons, plasmids were prepared by EndoFree plasmid kit (Qiagen)

Table 1
Primers for truncated δ-catenin

Construct name	Primers
DI321440	5′-ATCGTCGTGTCCTCGCCTCTGCCGCCAGCA-3′ 5′-TGCTGGCGGCAGAGGCGAGGACACGACGAT-3′
DI321420	5′-ATCGTCGTGTCCTCGTATGAAGACCGTGTC-3′ 5′-GACACGGTCTTCATACGAGGACACGACGAT-3′
DI321350	5′-ATCGTCGTGTCCTCGGGCACCTACGCCACC-3′ 5′-GGTGGCGTAGGTGCCCGAGGACACGACGAT-3′
DI351390	5′-CTGAGCTCCACCATCGGATCCCGAGCCTCG-3′ 5′-CGAGGCTCGGGATCCGATGGTGGAGCTCAG-3′
DI391435	5′-GGCAGCCTGGCAGCTCAGAGCCAGGGGGAT-3′ 5′-ATCCCCCTGGCTCTGAGCTGCCAGGCTGCC-3′
DI457468	5′-ACGAGCACAGCCCCGGGCAGCCAACACGGG-3′ 5′-CCCGTGTTGGCTGCCCGGGGCTGTGCTCGT-3′
DI462463	5′-TCCTCCCCTGGTGTCGTCCCCTTGCAGCGC-3′ 5′-GCGCTGCAAGGGGACGACACCAGGGGAGGA-3′
DI441480	5′-CAGAGCCAGGGGGATGCCACCTTCCAGAGG-3′ 5′-CCTCTGGAAGGTGGCATCCCCCTGGCTCTG-3′
DI450455	5′-GCACATACCGGCACCCCGTCCTCCCCTGGT-3′ 5′-ACCAGGGGAGGACGGGGTGCCGGTATGTGC-3′
DI421430	5′-CACATAGACCCCATCATGAGGAGTCTCAGC-3′ 5′-GCTGAGACTCCTCATGATGGGGTCTATGTG-3′
DI431450	5′-TATCAGAAGCCCCCTCGCACGAGCACAGCC-3′ 5′-GGCTGTGCTCGTGCGAGGGGGCTTCTGATA-3′
DI351370	5′-CTGAGCTCCACCATCAAGCATTCGCAGGAG-3′ 5′-CTCCTGCGAATGCTTGATGGTGGAGCTCAG-3′
DI371390	5′-TCTGAGCAGTACAGCGGATCCCGAGCCTCG-3′ 5′-CGAGGCTCGGGATCCGCTGTACTGCTCAGA-3′
DI391420	5′-GGCAGCCTGGCAGCTTATGAAGACCGTGTC-3′ 5′-GACACGGTCTTCATAAGCTGCCAGGCTGCC-3′

and Plasmid Plus kit (Qiagen) to minimize the endotoxin level. For HEK cells, plasmids prepared by HiSpeed plasmid kits (Qiagen) were also included. All the media were changed 1 day after transfection for HEK cells, and half of the media were changed 4–8 h after transfection for neurons.

Plasmids

The cDNA construct with the long isoform of mouse δ-catenin (Uniprot identifier, O35927-1) was a generous gift from Dr. Werner Franke (German Cancer Research Center, Germany) (4). The enhanced GFP–δ-catenin construct carries the short isoform of mouse δ-catenin (Uniprot identifier, O35927-2) and was a generous gift from Dr. Shernaz Bamji (University of British Columbia) (9). The δ-cat shRNA and the shRNA-resistant δ-catenin construct based on the mouse long isoform were described previously (8). The pSuper GFP vector was used as a control for the δ-cat shRNA. TAP–δ-catenin was generated by the Mouse Genome Engineering core facility of University of Nebraska Medical Center. It carries the long isoform of mouse δ-catenin with its N terminus fused with a TAP tag, Myc–TEV-linker–His-tag, cloned into the pcDNA3.1 vector.

All the truncated δ-catenin were generated by GeneArt site-directed mutagenesis system (ThermoFisher Scientific, A13282) with AccuPrime *Pfx* DNA Polymerase (ThermoFisher Scientific, 12344040) and corresponding primers (Table 1) according to the manufacturer's protocol using shRNA-resistant δ-catenin cDNA construct as template. It is worth mentioning that the DNA sequence encoding ~200–300 amino acids in δ-catenin has a very high GC content, and therefore ≥4% DMSO was included during PCR. All the truncation sites were confirmed by Sanger sequencing.

Pharmacological reagents

Pharmacological reagents for neuron treatments are listed: D-AP5 (Tocris, 0106); (+)-MK801 (Tocris, 0924); CNQX (Tocris, 1045); ALLN (Sigma, A6185); MDL28170 (Sigma, M6690); MG132 (Sigma, M7449); tetrodotoxin (Tocris, 1069); lactacystin (Calbiochem, 426100); and bafilomycin A1 (Tocris, 1334). CA-074 Me was a generous gift from Dr. Huangui Xiong (University of Nebraska Medical Center). Thapsigargin was a generous gift from Dr. Keshore Bidasee (University of Nebraska Medical Center). Cortical neurons were treated between DIV 10 and 28. Before treatment, the volume of the medium was measured to ensure no variability due to evaporation. Control samples were treated with same volume of H_2O or DMSO accordingly.

Ca^{2+}-free medium was prepared from Ca^{2+}- and Mg^{2+}-free Hanks' balanced salt solution (ThermoFisher Scientific, 14170112) supplemented with 0.814 mM $MgCl_2$, 10 mM HEPES, and extra 24.4 mM D-glucose and then equilibrant with 5% CO_2 at 37 °C. Neurons were incubated in Ca^{2+}-free medium for 10–15 min before treatment. $CaCl_2$ (1.8 mM final concentration) was mixed with NMDA/vehicle immediately before adding to the cells. The final concentrations of Mg^{2+} and Ca^{2+} were identical to the maintenance medium. For KCl treatment, an extra 55 mM KCl was added to the maintenance medium for a final concentration of 60.33 mM, and the control group was treated with same volume of water.

Lysate preparation and immunoblotting

For brain tissue collection, animals were anesthetized by isoflurane, and then brains were dissected in cold 1× PBS on ice. Brain tissues were quick frozen on dry ice and stored at −80 °C. Because δ-catenin in the brain tissue is susceptible to cleavage during the freeze-thaw cycle (data not shown), cold lysis buffer was added before thawing the tissue on the ice. 100–1000 μl of cold lysis buffer was used depending on the size of the tissue. Lysis buffer includes 1:100 proteinase inhibitor (Sigma, P8340) and 1:100 phosphatase inhibitor (Sigma, P0044) in the RIPA buffer (50 mM Tris (pH 7.4), 107 mM NaCl, 1% Triton X-100, 0.1% SDS). Besides the *in vitro* cleavage assay, all lysis buffer included 5 mM EDTA and an extra 5 mM EGTA for neuron or tissue. Brain tissues were homogenized for 2 s on ice by sonicator (22–25% amplitude) 3–8 times depending on the size of the tissue, with minimally a 60-s interval between rounds.

Before neuron lysis, cells were washed with cold 1× PBS. HEK cells were lysed without washing because they tend to detach. 70–100 μl of cold lysis buffer was added per well in a 6-well plate. After being scraped off by a cold cell scraper, cells were first pipetted up and down for about 30 times, then sheared with a cold 26/27-gauge needle for about 30 times. All the procedures were done on ice.

All the lysates were centrifuged 15,000 rpm for 15 min at 4 °C, then quick frozen on dry ice, and stored at −80 °C. Supernatants were mixed with Laemmli buffer and loaded on the gel (30–50 μg/well). For DcatCTI/II detection in neural lysate, 50 μg/well was optimal. Both hand-casted and precasted gels (Bio-Rad, 456-1084 and 456-1024) were used for SDS-PAGE. To separate DcatCTI/II and DcatNTI/II, 7.5–8 and 10% gels were

used, respectively. For separating DcatCTI and II from neural lysate, we had to run the gels longer making β-tubulin unusable as a housekeeping marker. In such case, we used Na^+/K^+-ATPase as a loading control.

Dilution of antibodies for immunoblot are as follows: 1:900 TL (BD Biosciences, 611537); 1:50 J19 (Progen, 651152); 1:100–1:500 β-tubulin (DHSB, E7); 1:200 actin (DHSB, JLA20); 1:400 Na^+/K^+-ATPase (DHSB, a6F); 1:5000 N-cadherin (BD Biosciences, 610920); 1:1000 PSD95 (Millipore, MAB1598); 1:2000 CaMKIIα (Millipore, 6G905-532); 1:1000 GAPDH (ThermoFisher Scientific, PA1-988); 1:4000 αII-spectrin (clone AA6, Enzo, BML-FG6090); 1:16,000 HRP-conjugated anti-rabbit IgG (Jackson ImmunoResearch, 711-035-152); and 1:16,000 HRP-conjugated anti-mouse IgG (Jackson ImmunoResearch, 711-035-151). 587 is a custom-made polyclonal rabbit antibody from ThermoFisher Scientific. It targets SELNYETSHYPASPDSWV of δ-catenin and was purified with GST fusion protein. Myc antibody (clone 9E10) was produced by the core facility of University of Nebraska Medical Center. ARVCF antibody was a generous gift from Dr. Keith Johnson (University of Nebraska Medical Center).

Blots were detected by SuperSignal West Dura chemiluminescent substrate (ThermoFisher Scientific, 34076) and imaged by FluorChem HD2 (Cell Biosciences). All the blots were quantified by AlphaView (ProteinSimple) or ImageJ. The sum signal of each band/isoform was subtracted by the sum background signal of the similarly sized selection area. All the protein quantifications were normalized to a housekeeping protein shown in the blot.

In vitro cleavage assay

As described earlier, the *in vitro* assay is identical to the lysate preparation except for exclusion of chelator in the lysis buffer. For inhibitor testing (Fig. 2*D*), inhibitor or vesicle was mixed with lysis buffer immediately before adding to the cells. However, because CA-074 Me needs to be hydrolyzed by intracellular enzyme for irreversible inhibition of cathepsin B, cells were pretreated with CA-074 Me instead of directly mixing the inhibitor with lysis buffer.

Calculate molecular weight

The molecular weight measurement was done in AlphaView and refers to protein ladders from Bio-Rad (1610394/1610393). Only lanes right next to the protein ladder were used for measuring molecular weight to ensure accuracy. Molecular weights for DcatNT and DcatCT were measured on blots probing with J19 and 587, respectively. Because the band of DcatNTII was thick, the molecular weight of DcatNTII was represented by the higher border of band.

The molecular weight of DcatCTII from both NMDA- and glutamate-treated samples were pooled to represent DcatCTII in neuron. Moreover, because the sample beside the ladder was always control, often having only DcatI ($DcatI_{Ctrl}$), we thus calculated DcatII as in Equation 1,

$$DcatII = DcatCTI_{Ctrl} - (DcatCTI_{NMDA/Glut} - DcatCTII_{NMDA/Glut}) \quad \text{(Eq. 1)}$$

$DcatCTI_{NMDA/Glut}$ and $DcatCTII_{NMDA/Glut}$ are the DcatCTI and CTII from the NMDA- or glutamate-treated samples, respectively.

δ-Catenin purification

TAP–δ-catenin in HEK cells were purified by PureProteom magnetic protein A/G beads (Millipore, LSKMAGA02/LSKMAGG02) according to the manufacturer's protocol with some modifications. The beads were cross-linked to Myc antibody and then blocked with 5% BSA. The fresh lysate was incubated with precleared beads on a rotator at 4 °C overnight. After washing with lysis buffer (a different protease inhibitor was used: ThermoFisher Scientific 88266), the TAP–δ-catenin were eluted with glycine (pH 2.5). Elution was immediately neutralized by Tris buffer (pH 8.0) and then stored at −80 °C. Independent batch of purified δ-catenin was used for each independent experiment.

For *in vitro* cleavage using purified δ-catenin, fresh lysate was prepared from nontransfected HEK cells and mixed with purified δ-catenin at 4 °C for 1 h. The reaction was stopped by adding Laemmli buffer to the samples. For heat inactivation, lysate was incubated at 80 °C for 10 min before the reaction.

Immunocytochemistry and microscopy

Briefly, coverslips were fixed in warm (37 °C) fixation buffer with 4% paraformaldehyde and 4% sucrose in 1× PBS for 20 min. 10 min of 0.1% Triton X-100 was used for permeabilization. Images were taken by LSM 700 confocal microscope (Zeiss) with 2048 × 2048 dpi, 8 bit, zoom 2, speed 6, 9 stacks with 0.47-μm interval. The expression of full-length or calpain-resistant δ-catenin in knockdown neurons was confirmed by immunostaining with δ-catenin. Dendritic protrusions from the thickest dendrite from each neuron was measured. All the protrusions located more than 10 μm from the soma were manually analyzed in Z-stack in ImageJ. All the analyses were done blind to the experimental groups.

Statistics

Statistics tests were performed in Prism 7 (GraphPad) and MATLAB. D'Agostino and Pearson normality tests were performed for all the data, and parametric/nonparametric test was performed accordingly. Data with too few numbers for the normality test were treated as normal distributions. n represents the number of independent experiments. CI was calculated as 95% confidence interval. Two-tailed p value was calculated accordingly, and significance level was 0.05. $0.05 \geq p > 0.01$: indicated by number in each panel; **, $p \leq 0.01$, ***, $p \leq 0.001$; ****, $p \leq 0.0001$.

Immunoblot and morphology analysis

Quantification for different brain regions (Fig. 1*B*) was first normalized to β-tubulin and then normalized to the average DcatCT or -NT level of five brain regions in the same mouse to reduce the data to independent observations (43).

For analysis of pharmacological treatments, the treatment groups were paired to the control sample of the experiment. Moreover, the effect of treatment was measured by ratio

instead of difference, compared with the control; thus, the results were log transformed before statistical analysis. Analysis of MK801 and CNQX treatment (Fig. 4, *F–H*), due to the null hypothesis, is "the treatment affects the level of DcatCT/NT/SBDP"; thus, correction for false positive is not applicable in this case. For repeated measure two-way ANOVA, data were presented by mean ± CI to accurately represent the relationship of data across groups in different tests.

For morphology analysis, all the data points were normalized to the geometric mean/median of the vector group of the experiment so that unpaired tests could be performed. Because the data were nonparametric the distributed and rank-based test would be performed; thus, they were not transformed to logarithmic scale.

Fraction and approximate density for each population

Because not all the protrusions were measured for width and length due to some of the protrusions overlapping with each other, the fraction for each population in each dendrite was calculated from the total number of P_n protrusions measured as shown in Equation 2,

$$P_n \text{ fraction} = \frac{\text{Number of } P_n}{\text{Number of } (P_1 + P_2 + P_3)} \quad \text{(Eq. 2)}$$

where $n = 1$, 2, or 3.

The approximate density was used to represent the density for the population as shown in Equation 3.

$$\text{Approximate } P_n \text{ density} = P_n \text{ fraction} \times \text{protrusion density} \quad \text{(Eq. 3)}$$

Because of a few dendrites in the vector group having no protrusion from a certain population, P_n fraction or approximate density was normalized to the median of the vector group in each experiment.

Determine P1 density threshold

Probability frequency was estimated by Kernel smoothing function. To better visualize the distribution of the data, estimation was calculated by bootstrapping with replacement for 500 times. The threshold was drawn according to the distribution difference basing on the criteria mentioned above.

Above threshold fraction comparison

Above threshold fraction for each group was calculated from bootstrap with replacement for 5000 times. The difference between each group and the knockdown sample, (each group, δ-cat shRNA), in each resampling was calculated, and the p value was equal to the number of (difference ≥ 0) divided by 5000. The stack of five p value were then corrected by Bonferroni-Dunn correction.

Author contributions—L. Y. and J. A. conceptualization; L. Y. data curation; L. Y. formal analysis; L. Y. validation; L. Y., D. S., and J. A. investigation; L. Y. visualization; L. Y. and J. A. methodology; L. Y. and J. A. writing-original draft; D. S., J. L. B., and J. A. resources; J. A. supervision; J. A. funding acquisition; J. A. project administration.

Acknowledgments—We thank R. Quadros and C. Gurumurthy for the TAP–δ-catenin and A. Suresh for the helpful discussions.

References

1. Penzes, P., Cahill, M. E., Jones, K. A., VanLeeuwen, J.-E., and Woolfrey, K. M. (2011) Dendritic spine pathology in neuropsychiatric disorders. *Nat. Neurosci.* **14,** 285–293 CrossRef Medline
2. Bourgeron, T. (2015) From the genetic architecture to synaptic plasticity in autism spectrum disorder. *Nat. Rev. Neurosci.* **16,** 551–563 CrossRef Medline
3. Seong, E., Yuan, L., and Arikkath, J. (2015) Cadherins and catenins in dendrite and synapse morphogenesis. *Cell Adh. Migr.* **9,** 202–213 CrossRef Medline
4. Paffenholz, R., and Franke, W. W. (1997) Identification and localization of a neurally expressed member of the plakoglobin/armadillo multigene family. *Differentiation* **61,** 293–304 CrossRef Medline
5. Gu, D., Sater, A. K., Ji, H., Cho, K., Clark, M., Stratton, S. A., Barton, M. C., Lu, Q., and McCrea, P. D. (2009) *Xenopus* δ-catenin is essential in early embryogenesis and is functionally linked to cadherins and small GTPases. *J. Cell Sci.* **122,** 4049–4061 CrossRef Medline
6. Kawamura, Y., Fan, Q. W., Hayashi, H., Michikawa, M., Yanagisawa, K., and Komano, H. (1999) Expression of the mRNA for two isoforms of neural plakophilin-related arm-repeat protein/δ-catenin in rodent neurons and glial cells. *Neurosci. Lett.* **277,** 185–188 CrossRef Medline
7. Arikkath, J., Israely, I., Tao, Y., Mei, L., Liu, X., and Reichardt, L. F. (2008) Erbin controls dendritic morphogenesis by regulating localization of δ-catenin. *J. Neurosci.* **28,** 7047–7056 CrossRef Medline
8. Arikkath, J., Peng, I. F., Ng, Y. G., Israely, I., Liu, X., Ullian, E. M., and Reichardt, L. F. (2009) δ-Catenin regulates spine and synapse morphogenesis and function in hippocampal neurons during development. *J. Neurosci.* **29,** 5435–5442 CrossRef Medline
9. Brigidi, G. S., Sun, Y., Beccano-Kelly, D., Pitman, K., Mobasser, M., Borgland, S. L., Milnerwood, A. J., and Bamji, S. X. (2014) Palmitoylation of δ-catenin by DHHC5 mediates activity-induced synapse plasticity. *Nat. Neurosci.* **17,** 522–532 CrossRef Medline
10. Ochiishi, T., Futai, K., Okamoto, K., Kameyama, K., and Kosik, K. S. (2008) Regulation of AMPA receptor trafficking by δ-catenin. *Mol. Cell. Neurosci.* **39,** 499–507 CrossRef Medline
11. Matter, C., Pribadi, M., Liu, X., and Trachtenberg, J. T. (2009) δ-Catenin is required for the maintenance of neural structure and function in mature cortex *in vivo*. *Neuron* **64,** 320–327 CrossRef Medline
12. Yuan, L., and Arikkath, J. (2017) Functional roles of p120ctn family of proteins in central neurons. *Semin. Cell Dev. Biol.* **69,** 70–82 CrossRef Medline
13. Abu-Elneel, K., Ochiishi, T., Medina, M., Remedi, M., Gastaldi, L., Caceres, A., and Kosik, K. S. (2008) A δ-catenin signaling pathway leading to dendritic protrusions. *J. Biol. Chem.* **283,** 32781–32791 CrossRef Medline
14. Kim, H., Han, J. R., Park, J., Oh, M., James, S. E., Chang, S., Lu, Q., Lee, K. Y., Ki, H., Song, W. J., and Kim, K. (2008) δ-Catenin-induced dendritic morphogenesis. An essential role of p190RhoGEF interaction through Akt1-mediated phosphorylation. *J. Biol. Chem.* **283,** 977–987 CrossRef Medline
15. Israely, I., Costa, R. M., Xie, C. W., Silva, A. J., Kosik, K. S., and Liu, X. (2004) Deletion of the neuron-specific protein δ-catenin leads to severe cognitive and synaptic dysfunction. *Curr. Biol.* **14,** 1657–1663 CrossRef Medline
16. Turner, T. N., Sharma, K., Oh, E. C., Liu, Y. P., Collins, R. L., Sosa, M. X., Auer, D. R., Brand, H., Sanders, S. J., Moreno-De-Luca, D., Pihur, V., Plona, T., Pike, K., Soppet, D. R., Smith, M. W., *et al.* (2015) Loss of δ-catenin function in severe autism. *Nature* **520,** 51–56 CrossRef Medline
17. Medina, M., Marinescu, R. C., Overhauser, J., and Kosik, K. S. (2000) Hemizygosity of δ-catenin (CTNND2) is associated with severe mental retardation in cri-du-chat syndrome. *Genomics* **63,** 157–164 CrossRef Medline
18. Belcaro, C., Dipresa, S., Morini, G., Pecile, V., Skabar, A., and Fabretto, A. (2015) CTNND2 deletion and intellectual disability. *Gene* **565,** 146–149 CrossRef Medline

19. Lee, M. S., Kwon, Y. T., Li, M., Peng, J., Friedlander, R. M., and Tsai, L.-H. (2000) Neurotoxicity induces cleavage of p35 to p25 by calpain. *Nature* **405,** 360–364 CrossRef Medline
20. Bai, G., and Pfaff, S. L. (2011) Protease regulation: the yin and yang of neural development and disease. *Neuron* **72,** 9–21 CrossRef Medline
21. Bingol, B., and Sheng, M. (2011) Deconstruction for reconstruction: the role of proteolysis in neural plasticity and disease. *Neuron* **69,** 22–32 CrossRef Medline
22. Ono, Y., Saido, T. C., and Sorimachi, H. (2016) Calpain research for drug discovery: challenges and potential. *Nat. Rev. Drug Discov.* **15,** 854–876 CrossRef Medline
23. Harris, D. C. (2010) *Quantitative Chemical Analysis*, 8th Ed., W. H. Freeman & Co., New York
24. Amini, M., Ma, C. L., Farazifard, R., Zhu, G., Zhang, Y., Vanderluit, J., Zoltewicz, J. S., Hage, F., Savitt, J. M., Lagace, D. C., Slack, R. S., Beique, J.-C., Baudry, M., Greer, P. A., Bergeron, R., and Park, D. S. (2013) Conditional disruption of calpain in the CNS alters dendrite morphology, impairs LTP, and promotes neuronal survival following injury. *J. Neurosci.* **33,** 5773–5784 CrossRef Medline
25. Vosler, P. S., Brennan, C. S., and Chen, J. (2008) Calpain-mediated signaling mechanisms in neuronal injury and neurodegeneration. *Mol. Neurobiol.* **38,** 78–100 CrossRef Medline
26. Yoshimori, T., Yamamoto, A., Moriyama, Y., Futai, M., and Tashiro, Y. (1991) Bafilomycin A1, a specific inhibitor of vacuolar-type H^+-ATPase, inhibits acidification and protein degradation in lysosomes of cultured cells. *J. Biol. Chem.* **266,** 17707–17712 Medline
27. Haggie, P. M., and Verkman, A. S. (2009) Unimpaired lysosomal acidification in respiratory epithelial cells in cystic fibrosis. *J. Biol. Chem.* **284,** 7681–7686 CrossRef Medline
28. Martinez, J. A., Zhang, Z., Svetlov, S. I., Hayes, R. L., Wang, K. K., and Larner, S. F. (2010) Calpain and caspase processing of caspase-12 contribute to the ER stress-induced cell death pathway in differentiated PC12 cells. *Apoptosis* **15,** 1480–1493 CrossRef Medline
29. Zhou, Q., Petersen, C. C., and Nicoll, R. A. (2000) Effects of reduced vesicular filling on synaptic transmission in rat hippocampal neurones. *J. Physiol.* **525,** 195–206 CrossRef Medline
30. Hering, H., and Sheng, M. (2001) Dendritic spines: structure, dynamics and regulation. *Nat. Rev. Neurosci.* **2,** 880–888 CrossRef Medline
31. Luzio, J. P., Pryor, P. R., and Bright, N. A. (2007) Lysosomes: fusion and function. *Nat. Rev. Mol. Cell Biol.* **8,** 622–632 CrossRef Medline
32. Ide, N., Hata, Y., Deguchi, M., Hirao, K., Yao, I., and Takai, Y. (1999) Interaction of S-SCAM with neural plakophilin-related armadillo-repeat protein/δ-catenin. *Biochem. Biophys. Res. Commun.* **256,** 456–461 CrossRef Medline
33. Silverman, J. B., Restituito, S., Lu, W., Lee-Edwards, L., Khatri, L., and Ziff, E. B. (2007) Synaptic anchorage of AMPA receptors by cadherins through neural plakophilin-related arm protein AMPA receptor-binding protein complexes. *J. Neurosci.* **27,** 8505–8516 CrossRef Medline
34. Jones, S. B., Lanford, G. W., Chen, Y. H., Moribito, M., Kim, K., and Lu, Q. (2002) Glutamate-induced δ-catenin redistribution and dissociation from postsynaptic receptor complexes. *Neuroscience* **115,** 1009–1021 CrossRef Medline
35. Lu, Q., Paredes, M., Medina, M., Zhou, J., Cavallo, R., Peifer, M., Orecchio, L., and Kosik, K. S. (1999) δ-Catenin, an adhesive junction-associated protein which promotes cell scattering. *J. Cell Biol.* **144,** 519–532 CrossRef Medline
36. Gu, D., Tonthat, N. K., Lee, M., Ji, H., Bhat, K. P., Hollingsworth, F., Aldape, K. D., Schumacher, M. A., Zwaka, T. P., and McCrea, P. D. (2011) Caspase-3 cleavage links δ-catenin to the novel nuclear protein ZIFCAT. *J. Biol. Chem.* **286,** 23178–23188 CrossRef Medline
37. Markham, N. O., Doll, C. A., Dohn, M. R., Miller, R. K., Yu, H., Coffey, R. J., McCrea, P. D., Gamse, J. T., and Reynolds, A. B. (2014) DIPA-family coiled-coils bind conserved isoform-specific head domain of p120-catenin family: potential roles in hydrocephalus and heterotopia. *Mol. Biol. Cell.* **25,** 2592–2603 CrossRef Medline
38. López-Otín, C., and Matrisian, L. M. (2007) Emerging roles of proteases in tumour suppression. *Nat. Rev. Cancer* **7,** 800–808 CrossRef Medline
39. Papa, M., Bundman, M. C., Greenberger, V., and Segal, M. (1995) Morphological analysis of dendritic spine development in primary cultures of hippocampal neurons. *J. Neurosci.* **15,** 1–11 CrossRef Medline
40. Harris, K. M. (1999) Structure, development, and plasticity of dendritic spines. *Curr. Opin. Neurobiol.* **9,** 343–348 CrossRef Medline
41. Suresh, A., and Dunaevsky, A. (2017) Relationship between synaptic AMPAR and spine dynamics: impairments in the FXS mouse. *Cereb. Cortex* **27,** 4244–4256 CrossRef Medline
42. Beaudoin, G. M., 3rd., Lee, S. H., Singh, D., Yuan, Y., Ng, Y. G., Reichardt, L. F., and Arikkath, J. (2012) Culturing pyramidal neurons from the early postnatal mouse hippocampus and cortex. *Nat. Protoc.* **7,** 1741–1754 CrossRef Medline
43. Valcu, M., and Valcu, C.-M. (2011) Data transformation practices in biomedical sciences. *Nat. Methods* **8,** 104–105 CrossRef Medline